Letter

Structure factor and topological bound of twisted bilayer semiconductors at fractional fillings

Timothy Zaklama,[1,*] Di Luo,[1,2,3] and Liang Fu[1,†]

[1]*Department of Physics, Massachusetts Institute of Technology, Cambridge, Massachusetts 02139, USA*

[2]*The NSF AI Institute for Artificial Intelligence and Fundamental Interactions, Cambridge, Massachusetts 02139, USA*

[3]*Department of Physics, Harvard University, Cambridge, Massachusetts 02138, USA*

(Received 11 November 2024; revised 27 February 2025; accepted 17 June 2025; published 14 July 2025)

The structure factor is a useful observable for probing charge density correlations in real materials, and its long-wavelength behavior encapsulated by "quantum weight" has recently gained prominence in the study of quantum geometry and topological phases of matter. Here, we employ the full static structure factor $S(\mathbf{q})$ to explore the phase diagram of twisted transition metal dichalcogenides (TMDs), specifically $t\mathrm{MoTe}_2$, at filling factors $\nu = 1/3, 2/3$ under varying displacement fields. Our results reveal a topological phase transition between a fractional Chern insulator (FCI) and a generalized Wigner crystal. This transition is marked by the appearance of Bragg peaks at charge-density-wave vectors, and simultaneously, a large decrease of $S(\mathbf{q})$ at small $\mathbf{q}$ which lowers the interaction energy. We further calculate the quantum weight of various FCI states, verifying the universal topological bound for interacting systems. Our findings provide insights into the phase diagram of twisted TMDs and establish a general framework for characterizing topological phases through structure factor analysis.

DOI: 10.1103/wlvf-tdq1

Introduction. The structure factor is a fundamental quantity for probing the crystal structure and charge/spin density fluctuations in real materials, which can be measured by x-ray diffraction, electron loss spectroscopy, and neutron scattering. In particular, the static (or equal-time) structure factor $S(\mathbf{q})$ is a ground-state property defined as the Fourier transform of a spatial density correlation. In periodic solids, Bragg peaks in the structure factor identify crystal structures and charge-density-wave orders [1]. In quantum liquids, the static structure factor encodes useful information about the ground state and excitation spectrum [2]. For example, the structure factor of helium exhibits a characteristic peak at the wave vector set by the inverse particle distance, which is closely related to the roton excitation [3].

Recently, the behavior of the structure factor $S(\mathbf{q})$ at small $\mathbf{q}$, which characterizes long-wavelength density correlations, has received growing attention. For gapped many-body systems, $S(\mathbf{q} \to 0)$ is generally quadratic in $\mathbf{q}$ and the quadratic coefficient K defines a fundamental ground-state property recently termed quantum weight [4,5]. Interestingly, quantum weight is directly related to optical response [5], charge fluctuation [6–8], and many-body quantum geometry [9]. It also sets an upper bound on the energy gap and a lower bound on the static dielectric constant of solids [5,10,11].

Very recently, a universal lower bound for quantum weight has been established for Chern insulators [12], $K \geqslant |C|$, where C is the many-body Chern number. This inequality is derived from the fundamental principles of physics and therefore applies generally to two-dimensional electron systems with either integral or fractional quantized Hall conductivity $\sigma_{xy} = Ce^2/h$, with or without magnetic field. The bound on quantum weight is saturated in (integer and fractional) quantum Hall states that occur in a two-dimensional electron gas under strong magnetic fields [1], whereas the opposite behavior $K \gg |C| = 1$ is found for the magnetic topological insulator $\mathrm{MnBi_2Te_4}$ [13].

For noninteracting band insulators, the quantum weight K is directly related to the spread of Wannier functions in real space [14]. Narrow-gap semiconductors have more extended Wannier functions and therefore larger K. For a Chern band, the bound $K \geqslant |C|$ dictates that the corresponding Wannier functions must have a minimum spread that is given by C times the lattice constant. More generally, the quantum weight of interacting two-dimensional systems is directly related to many-body quantum geometry, which is defined by the ground-state wave function over twisted boundary conditions [9,15]. While the geometry of Chern bands has been intensively studied in recent years [16–23], little is known about the many-body quantum geometry of fractional Chern insulators (FCIs).

In this Letter, we use band-projected exact diagonalization (ED) to calculate the full structure factor of twisted homobilayer transition metal dichalcogenides (TMDs) at various fractional fillings and displacement fields. Small-twist-angle bilayer TMDs host flat Chern bands [24,25], which can enable robust ferromagnetism and a fractional quantum anomalous Hall effect at fractional band fillings [26,27]. Recent experiments on twisted bilayer $\mathrm{MoTe_2}$ have revealed a sequence of FCIs at zero magnetic field [28–30], which bears a remarkable similarity to the Jain sequence fractional quantum Hall states in the lowest Landau level [31–41]. Unlike the latter, however, theory predicts that $t\mathrm{MoTe_2}$ also hosts generalized

*Contact author: tzaklama@mit.edu

†Contact author: liangfu@mit.edu

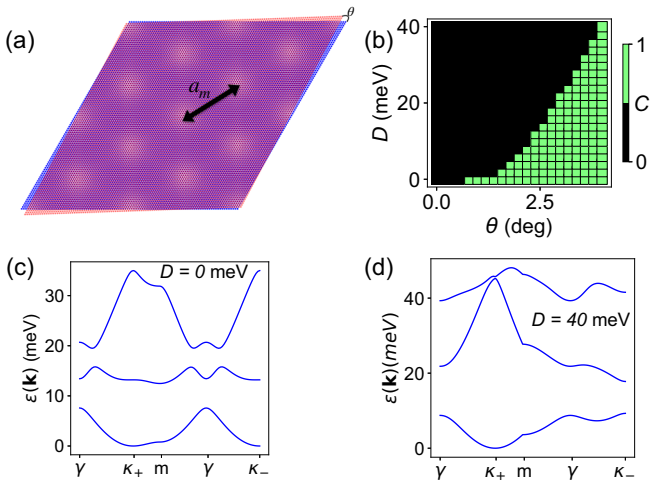

FIG. 1. Schematics and single-particle picture. (a) Schematic of the emergent moiré superlattice in real space and (b) the single-particle Chern number as a function of the displacement field and twist angle. There is a clear trend that as the displacement field gets larger, one must go to a larger twist angle to expect topology. (c), (d) The continuum band structure for $\theta = 2.8^\circ$ and $D = 0, 40$ meV, respectively.

Wigner crystals (GWCs) [31,42–44], anomalous Hall metals [37], and quantum anomalous Hall crystals [45,46], leading to a fascinating phase diagram.

Based on the structure factor, we identify and distinguish FCIs and GWCs at $\nu = 1/3$ and $2/3$ fillings under small and large displacement fields, respectively. The displacement-field-induced topological phase transition between the FCI and GWC states at $\nu = 2/3$ is marked by an abrupt decrease of quantum weight below the topological bound, which occurs in tandem with the emergence of charge-density-wave (CDW) Bragg peaks in order to lower the interaction energy. Our work further reveals a magic angle where the topological bound for FCIs is nearly saturated and demonstrates the persistence of $\nu = 2/3$ FCI to larger twist angles where the quantum weight significantly exceeds the bound.

Moiré band structure and band topology. Our study is based on the interacting continuum model for holes in twisted TMD homobilayers schematically represented in Fig. 1(a). The single-particle Hamiltonian for spin-1/2 holes is given by [24]

$$\mathcal{H}_\uparrow = \begin{pmatrix} \frac{\hbar^2(-i\nabla-\kappa_+)^2}{2m^*} + \tilde{V}_+(\mathbf{r}) & t(\mathbf{r}) \\ t^\dagger(\mathbf{r}) & \frac{\hbar^2(-i\nabla-\kappa_-)^2}{2m^*} + \tilde{V}_-(\mathbf{r}) \end{pmatrix}, \quad (1)$$

while $\mathcal{H}_\downarrow$ is its time-reversal conjugate. Here, $\kappa_\pm = \frac{4\pi}{3a_M}(-\frac{\sqrt{3}}{2}, \pm\frac{1}{2})$ is introduced by rotational misalignment, with a_M the moiré period and m^* the effective mass. $V_\pm(\mathbf{r}) = -2V\sum_{i=1,3,5}\cos(\mathbf{g}_i\cdot\mathbf{r} + \phi_\pm) \mp \frac{D}{2}$ denotes the moiré potential on each layer, where D is the layer potential bias introduced by the displacement field, and $t(\mathbf{r}) = w(1 + e^{-i\mathbf{g}_2\cdot\mathbf{r}} + e^{-i\mathbf{g}_3\cdot\mathbf{r}})$ denotes the interlayer tunneling. The moiré reciprocal lattice vectors are $\mathbf{g}_i = \frac{4\pi}{\sqrt{3}a_M}[\cos(\frac{\pi(i-1)}{3}), \sin(\frac{\pi(i-1)}{3})]$ for $i = 1, \ldots, 6$, with $\phi_+ = -\phi_- = \phi$. We take the explicit forms of the parameters for tMoTe$_2$ from Ref. [31].

The displacement field tunes the dispersion, wave function, and topology of moiré bands [24,25]. A large displacement field polarizes charges to one layer, and thereby drives the moiré bands from topological ($C = 1$) to trivial ($C = 0$), as shown in Fig. 1(b). Figures 1(c) and 1(d) show the moiré band structure and the Chern number of the lowest band for two representative displacement fields $D = 0$ and 40 meV. This work will focus on the effect of displacement field on the ground state of twisted homobilayer TMDs at fractional fillings.

Band-projected exact diagonalization. The full continuum model Hamiltonian including the electron-electron interaction is given by

$$\boldsymbol{H} = \boldsymbol{H}_0 + \boldsymbol{V},$$
$$\boldsymbol{V} = \frac{1}{2}\sum_{\sigma,\sigma'}\int d\mathbf{r}d\mathbf{r}'\psi^\dagger_\sigma(\mathbf{r})\psi^\dagger_{\sigma'}(\mathbf{r}')V(\mathbf{r}-\mathbf{r}')\psi_{\sigma'}(\mathbf{r}')\psi_\sigma(\mathbf{r}), \quad (2)$$

where $\boldsymbol{H_0} = \sum_{\sigma=\uparrow,\downarrow}\int d\boldsymbol{r}\psi^\dagger_\sigma\mathcal{H}_\sigma\psi_\sigma$. Here, we use a long-range Coulomb interaction $V(\mathbf{r}) = \frac{e^2}{\epsilon r}$. By diagonalizing the one-body Hamiltonian $\boldsymbol{H}_0$, we obtain the band dispersion and Bloch wave function. Then, $\boldsymbol{H}$ can be rewritten in Bloch band basis as follows,

$$\tilde{\boldsymbol{H}} = \sum_{\sigma,n,\mathbf{k}}\epsilon_{\sigma,n}(\mathbf{k})c^\dagger_{\sigma,n,\mathbf{k}}c_{\sigma,n,\mathbf{k}} + \frac{1}{2}\sum_{\substack{\sigma,\sigma';\mathbf{k}'_1 \\ n_1,n_2,n_3,n_4; \\ \mathbf{k}'_2\mathbf{k}_1,\mathbf{k}_2}} V^{\sigma\sigma'}_{\mathbf{k}'_1\mathbf{k}'_2\mathbf{k}_1\mathbf{k}_2}c^\dagger_{\sigma_1,n_1,\mathbf{k}'_1}c^\dagger_{\sigma_2,n_3,\mathbf{k}'_2}c_{\sigma_2,n_4,\mathbf{k}_2}c_{\sigma_1,n_2,\mathbf{k}_1}, \quad (3)$$

where $c^\dagger_{\sigma,n,\mathbf{k}}$ creates a hole in a Bloch state at spin/valley σ, band n, and crystal momentum $\mathbf{k}$, which has a corresponding single-particle energy $\epsilon_{\sigma,n}(\mathbf{k})$. The Coulomb interaction matrix elements take on the Bloch basis representation $V^{\sigma\sigma'}_{\mathbf{k}'_1\mathbf{k}'_2\mathbf{k}_1,\mathbf{k}_2} \equiv \langle\mathbf{k}'_1\sigma;\mathbf{k}'_2\sigma'|\hat{V}|\mathbf{k}_1\sigma;\mathbf{k}_2\sigma'\rangle$.

To solve many-body ground states at fractional fillings $\nu < 1$ with exact diagonalization, we truncate the full Hilbert space to the subspace spanned by the lowest band, i.e., we only keep terms with $n_1 = n_2 = n_3 = n_4 = 1$ in Eq. (3). This band projection neglects band mixing with higher bands, which is accurate when the ratio of the characteristic Coulomb energy $\frac{e^2}{\epsilon a_M}$ to the moiré band gap is sufficiently small. While band mixing is quantitatively important for tMoTe$_2$, band-projected ED captures the essential physics of FCIs [38,39].

Further, we assume that the system at the range of fillings considered hereafter is fully spin polarized, as found by previous numerical studies [27,31,38]. Our ED calculation uses the charge-$U(1)$ and spatial translational symmetries to diagonalize within the common eigenspace of N_e and center-of-mass (c.m.) crystal momentum. The ED at $\nu = 1/3, 2/3$ is performed on a 27-unit cell cluster with C_6 symmetry using periodic boundary conditions, as done in previous studies of this system [37,39].

Structure factor and quantum weight. The structure factor is defined as the Fourier transform of the static density-density

correlation function,

$$\chi(\mathbf{r}_i, \mathbf{r}_j) = \langle \rho(\mathbf{r}_i)\rho(\mathbf{r}_j)\rangle = \frac{1}{A}\sum_{\mathbf{q}} e^{i\mathbf{q}(\mathbf{r}_j-\mathbf{r}_i)} S(\mathbf{q}), \quad (4)$$

where $S(\mathbf{q}) = \frac{1}{A}\langle \rho(\mathbf{q})\rho(-\mathbf{q})\rangle$ for general fermionic momentum-space density operators $\rho(\mathbf{q}) = \sum_{\mathbf{k}} f^{\dagger}_{\mathbf{k}} f_{\mathbf{k}+\mathbf{q}}$ in the *plane-wave* basis, $\langle \cdots \rangle$ denotes the expectation value over the many-body ground state, and system area $A = \frac{\sqrt{3}a_M^2 N}{2}$ for cluster size N. We take $S(\mathbf{q})$ over a single ground state rather than averaging over degenerate many-body ground states.

The structure factor defined above is the standard one, which applies to all electronic systems. In contrast, a different structure factor has been considered in the literature on quantum Hall states [47] and recently twisted TMDs [34,37,42,48,49], which is defined by the *projected density operator* in the Chern band instead of the bare density operator ρ. It is important to note that the projected structure factor differs from the standard one, even when band mixing is negligible. The difference between the two structure factors is evident from their contrasting behaviors at large $\mathbf{q}$. At $\mathbf{q} \to \infty$, the projected structure factor vanishes, while the standard one approaches 1. In this work, we study the standard structure factor of twisted TMDs, which has not been calculated before.

As a ground-state property, $S(\mathbf{q})$ can be computed with a variety of numerical methods including exact diagonalization, making it a powerful tool for probing strongly correlated and highly entangled systems. Recently, it was recognized that the long-wavelength behavior of the (standard) structure factor $S(\mathbf{q})$ is an important quantity of quantum many-body systems. For systems with an energy gap, $S(\mathbf{q} \to 0)$ takes the general form

$$S(\mathbf{q}) = \frac{K_{\alpha\beta}}{2\pi} q_\alpha q_\beta + \cdots, \quad (5)$$

where the summation over spatial indices α and β is implied. In an interacting system, the quantum weight can also be formulated in terms of the quantum geometric tensor for the many-body ground state under twisted boundary conditions [4]. Interestingly, the trace of K has a *universal* lower bound determined by the many-body Chern number C (or equivalently, the quantized Hall conductivity) [12]:

$$K \equiv K_{xx} + K_{yy} \geqslant |C|. \quad (6)$$

This bound is saturated in Landau levels of two-dimensional electron gas due to the Galilean invariance. For FCIs such as twisted TMDs at fractional fillings, it remains unknown how close the bound is to the actual quantum weight.

To calculate the structure factor in band-projected ED, we first transform the fermion operators $f_{\mathbf{k}'}$ indexed by spin σ, layer X, and *plane-wave* momentum $\mathbf{k}'$ to the fermion operators $c_{\sigma,n,\mathbf{k}}$ in band basis indexed by σ, band index n, *crystal momentum* $\mathbf{k}$, and reciprocal lattice vector $\mathbf{G}$ as

$$f_{\sigma,X,\mathbf{k}+\mathbf{G}} = \sum_n u_{\sigma,n;\mathbf{G},X}(\mathbf{k}) c_{\sigma,n,\mathbf{k}}, \quad (7)$$

where $u_{\sigma,n;\mathbf{G},X}$ are the Bloch wave functions obtained from solving the single-particle Hamiltonian. Then, the full static

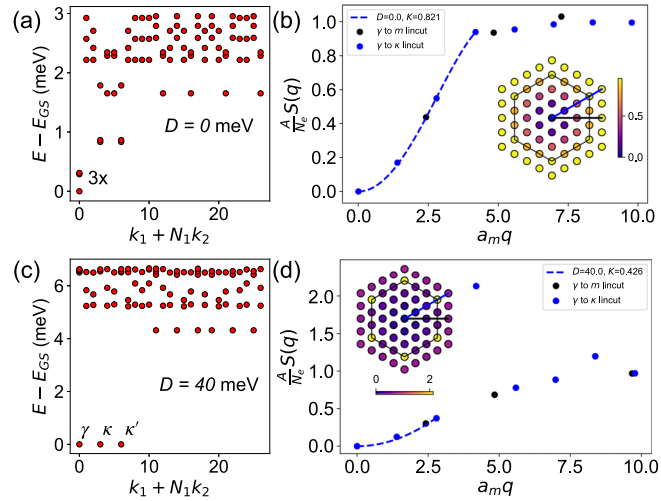

FIG. 2. FCI-to-GWC transition driven by displacement field. (a), (c) Many-body spectra on a 27-site cluster at $\nu = 2/3$, $\theta = 2.8°$, $\epsilon = 10$, and $D = 0, 40$ meV, respectively. There is a clear near-threefold degeneracy at γ for $D = 0$ meV that moves to γ, κ, κ' for $D = 40$ meV. (b), (d) γ to κ and γ to M linecut of $S(\mathbf{q})$ with the corresponding parameters of (a), (c). The insets in sub-panel (b) and (d) shows the full $S(\mathbf{q})$ one momentum shell outside of the Brillouin zone and the points according to their corresponding linecuts.

structure factor can be expressed solely in terms of the bands in which the many-body ground state resides, making numerical calculation far more tractable. The explicit calculation of the structure factor, along with its analytically simplified analog, is provided in the Supplemental Material [50].

Results. We now study the phase diagram of tMoTe$_2$ as the displacement field is turned on. Focusing first on $\nu = 2/3$ where the FCI state is most robust, we present in Fig. 2 the many-body spectra (MBS) (the energy spectrum partitioned by momentum sector) and ground-state structure factor for $D = 0$ and $D = 40$ meV, where the lowest moiré band is separated from remote bands and has $C = 1$ and $C = 0$, respectively. Calculations were done at a twist angle $\theta = 2.8°$ on an $N = 27$ cluster with a dielectric constant $\epsilon = 10$.

For $D = 0$, we find three nearly degenerate ground states in the same momentum sector, consistent with the previously identified FCI phase on this cluster geometry [31]. In contrast, for $D = 40$ meV, we find three degenerate ground states at distinct many-body momenta γ, κ, κ', which is consistent with a $\sqrt{3} \times \sqrt{3}$ GWC [43].

The emergence of GWC that spontaneously breaks lattice translation symmetry can be diagnosed by the structure factor. Indeed, for $D = 40$ meV, $S(\mathbf{q})$ shows a prominent peak at the expected wave vector. Moreover, the peak height is found to increase with system size, which demonstrates the presence of long-range charge-density-wave order, as shown in Figs. 3(c) and 3(d). The existence of $\sqrt{3} \times \sqrt{3}$ GWC is expected at large D, when charges reside on the MX moiré sites on one layer and form a honeycomb superstructure with a tripled unit cell to minimize the Coulomb repulsion, similar to the case of TMD heterobilayers [51]. In contrast, the structure factor of the FCI state at $D = 0$ is liquidlike and qualitatively similar to

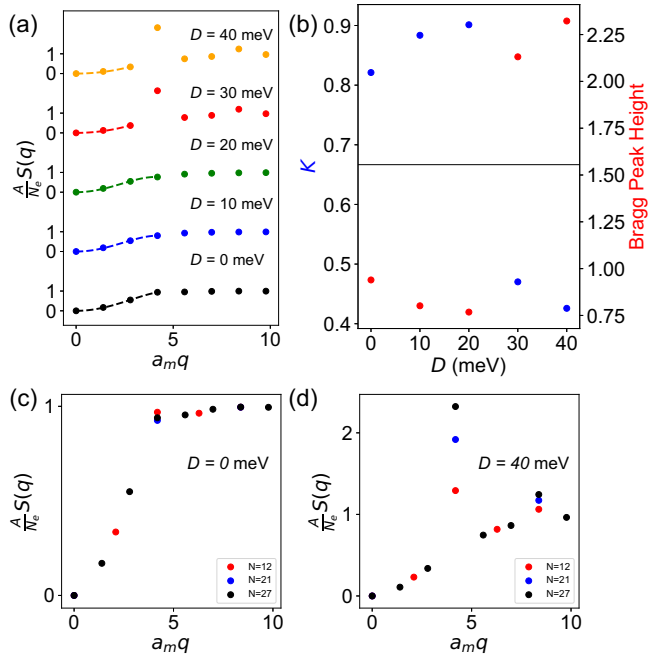

FIG. 3. $S(\mathbf{q})$ and quantum weight at various displacement fields for $\nu = 2/3$, $\theta = 2.8^\circ$, and $\epsilon = 10$. (a) $S(\mathbf{q})$ of the γ to κ linecut $S(\mathbf{q})$ vertically displaced to show dependence on the displacement field. Bragg peaks emerge at κ for $D = 30, 40$ meV and scale accordingly. (b) Quantum weight and $S(\mathbf{q})$ value of the κ, κ' Bragg peak vs the displacement field. (c), (d) $S(\mathbf{q})$ at increasing commensurate system size at $D = 0, 40$ meV, respectively. Bragg peaks emerge and scale as the system size in the GWC phase as expected.

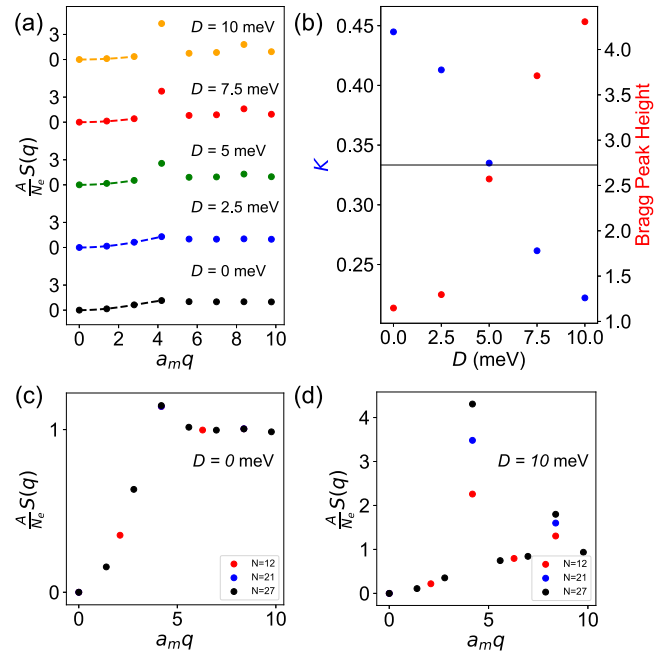

FIG. 4. $S(\mathbf{q})$ and quantum weight at various displacement fields for $\nu = 1/3$, $\theta = 2.0^\circ$, and $\epsilon = 10$. (a) $S(\mathbf{q})$ of the γ to κ linecut similar to Fig. 2. (b) Quantum weight and $S(\mathbf{q})$ value of the κ, κ' Bragg peak vs the displacement field. (c), (d) $S(\mathbf{q})$ at increasing commensurate system size at $D = 0, 10$ meV, respectively. Bragg peaks emerge and scale as the system size in the GWC phase as expected.

that of the $\nu = 2/3$ fractional quantum Hall state in the lowest Landau level.

We further analyze the structure factor $S(\mathbf{q})$ at small $\mathbf{q}$ and extract the quantum weight K by a quadratic fitting shown in Figs. 2(b) and 2(d) (see Supplemental Material for details [50]). We find $K = 0.821$ at $D = 0$, which indeed satisfies the universal topological bound of FCIs with $C = 2/3$. In contrast, at $D = 40$ meV, $K = 0.426$ falls below $2/3$, which rules out the possibility of a $C = 2/3$ FCI and instead is consistent with a topologically trivial state $C = 0$. Our structure factor analysis shows that quantum weight can provide a useful method to distinguish topological and trivial states using a single ground state.

We extend this analysis further to identify the phase transition from FCI to GWC as the displacement field D increases. Figure 3(a) shows $S(\mathbf{q})$ along the direction $\gamma - \kappa$ at increasing D. From $D = 0$ to 20 meV, $S(\mathbf{q})$ as a function of $\mathbf{q}$ increases smoothly from 0 to 1, characteristic of a quantum liquid. At $D = 30$ meV, a CDW Bragg peak arises abruptly and its magnitude increases further with D. Moreover, Fig. 3(b) shows that immediately when the Bragg peak develops, the K falls below $2/3$. Our findings provide strong evidence for a direct transition between FCI and GWC, which appears to be first order as evidenced by the discontinuity in quantum weight.

Experiments on $t\text{MoTe}_2$ have indeed observed at $\nu = 2/3$ a transition from FCI to a trivial insulating state ($\sigma_{xy} = 0$) under increasing displacement field [30]. The latter is consistent with the GWC, whose $\sqrt{3} \times \sqrt{3}$ charge order may be detected by scanning tunneling microscopy, or identified through different exciton energy shifts at inequivalent moiré sites in the tripled unit cell of the GWC.

We also study $t\text{MoTe}_2$ at $\nu = 1/3$. Previous numerical studies at $D = 0$ [31] have predicted that the $1/3$ state is a trivial $\sqrt{3} \times \sqrt{3}$ GWC at most of the twist angles, except in the neighborhood of a magic angle where the underlying Chern band is most lowest Landau level-like, giving rise to a $C = 1/3$ FCI. In this case, our calculations find a similar FCI-to-GWC transition under increasing displacement field, as shown in Fig. 4. Compared to $\nu = 2/3$, the FCI-to-GWC transition occurs at a smaller displacement field for $\nu = 1/3$.

It is worth noting that across the D-induced transition from FCI to GWC at $\nu = 2/3$ or $1/3$, the presence of Bragg peaks in the structure factor at the CDW wave vector is accompanied by a reduction of $S(\mathbf{q})$ at small $\mathbf{q}$, i.e., a decrease of quantum weight. This is not a coincidence and can be heuristically understood from energetic considerations as follows: The transition to the GWC is expected to lower the interaction energy, which is directly related to the structure factor, $E_{\text{int}} = \sum_{\mathbf{q}} V(\mathbf{q})(\frac{A}{N_e} S(\mathbf{q}) - 1)/2A$, where the Coulomb interaction $V(\mathbf{q}) = 2\pi e^2/\epsilon|\mathbf{q}|$ is positive at all $\mathbf{q}$, N_e is the number of electrons in the system, and A is the system area. On the other hand, the development of Bragg peaks in the GWC, however, indicates that $S(\mathbf{q})$ increases at the CDW wave vector. Therefore, the reduction of interaction energy can only be possible due to the decrease of $S(\mathbf{q})$ at other wave vectors, including small $\mathbf{q}$. We confirm the reduction

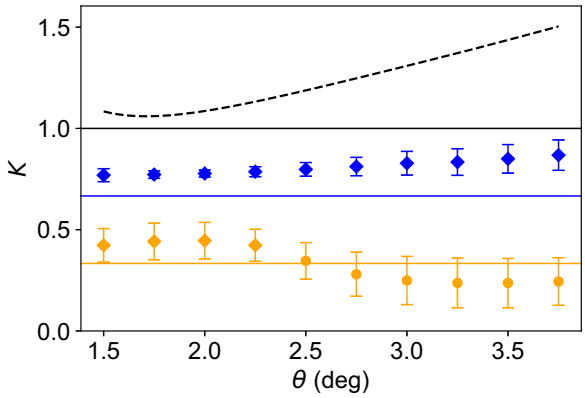

FIG. 5. Illustration of the universal topological bound being respected at fractional fillings. Extracted quantum weight is plotted vs twist angle at $\nu = 1/3, 2/3, 1$ (orange, blue, black, respectively). The universal topological bound for each filling is plotted as a solid horizontal line in the appropriate color, and the phase of the system at each angle is denoted by the style of the point. The diamonds correspond to points within the FCI phase, and the solid circles correspond to points within the GWC phase [31]. The dashed black line is the noninteracting case, previously shown to respect the topological bound in this system at integer filling [12]. All data are calculated at $\epsilon = 5$ and $D = 0$ on a 27-site cluster (error bars reflect the fit uncertainty due to finite-size effects).

of E_{int} across the FCI-to-GWC transition in the Supplemental Material [50].

Finally, we calculate the structure factor and extract the quantum weight at $D = 0$ as a function of twist angle for fillings $\nu = 1/3$ and $2/3$ in Fig. 5. For $\nu = 1/3$, the system transitions from an FCI to a GWC at $\theta \approx 2.4^\circ$, as indicated by the emergence of Bragg peaks, in agreement with the previous study [31]. As in the case of the displacement-field-induced FCI-GWC transition, we again see a fall in quantum weight below the topological bound across the phase boundary, signaling a topological phase transition. We find the mechanism for this shift is identical for the θ-induced FCI-GWC transition: The emergence of Bragg peaks increases $S(\mathbf{q})$ at the CDW wave vector, driving $S(\mathbf{q})$ down for small $\mathbf{q}$, forcing the quantum weight below the topological lower bound.

It is interesting to note that near the FCI-GWC phase boundary, the quantum weight nearly saturates the topological bound at a magic angle, which is around 2.4° for $\nu = 1/3$ and is less than 1.5° for $\nu = 2/3$. This is broadly consistent with the theoretical picture that the moiré band wave function at the magic angle closely resembles the lowest Landau level [25,35], and therefore the corresponding FCI states closely resemble the fractional quantum Hall states, whose quantum weight saturates the topological lower bound.

Perhaps more remarkable is that the $\nu = 2/3$ FCI persists to larger angles where the quantum weight far exceeds the topological bound. At $\theta = 3.75^\circ$, $K = 0.934$ is almost 3/2 times the topological bound signifying a considerable difference between this FCI state and the fractional quantum Hall state. It will be interesting to construct a variational wave function for such nonstandard FCI states featuring large quantum weight.

Discussion. In this Letter, we mapped out the phase diagram for $t\text{MoTe}_2$ at $\nu = 1/3$ and $2/3$ as a function of displacement field based primarily on the structure factor calculated by band-projected ED. We use $S(\mathbf{q})$ to distinguish liquid and crystal states, and uncover a displacement-field-induced topological phase transition using the quantum weight K. Our numerical results confirm the topological bound $K \geqslant |C|$ found by Oinishi and Fu for FCIs and identify the magic angle where this bound is nearly saturated.

We note that band-projected ED is quantitatively accurate when the band gap is large compared to the interaction energy. However, near the critical field where the band gap closes and band topology changes $C = 1 \to 0$, band mixing may affect the many-body ground states at fractional filling. Nonetheless, our band-projected ED provides variational ground-state energies and wave functions, which serve as a useful starting point and benchmark for further investigation with advanced numerical methods.

Our work has shown that the static structure factor encodes information about topological and correlated states in twisted TMDs. Further, our method is of broad and widespread application as it not only provides experimentalists with an additional tool to diagnose topology in real systems, but also theorists with a numerical means of measuring topology strictly from the ground-state wave function. Novel numerical methods such as neural network variational Monte Carlo that do not calculate excited states have particular use for our method. In practice, measuring $S(\mathbf{q})$ directly with conventional x-ray scattering techniques is an experimental challenge due to the ultrathin nature of 2D layers. In this regard, it is worth noting that the small-q behavior of $S(\mathbf{q})$ encapsulated by the quantum weight can be directly determined from terahertz optical conductivity using the sum rule [5],

$$K = 2\hbar \int_0^\infty d\omega \frac{\text{Re}\,\sigma_{xx}}{\omega}, \tag{8}$$

where the frequency integration should encompass the energy range of the continuum model for low-energy moiré bands.

Acknowledgments. We thank Yugo Onishi for a related collaboration and Aidan Reddy and Ahmed Abouelkomsan for helpful discussions. We also acknowledge the GitHub repository [52] that helped build the exact diagonalization and structure factor calculation code used in this work. This work was supported by the Air Force Office of Scientific Research under Award No. FA2386-24-1-4043. T.Z. was supported by the MIT Dean of Science Graduate Student Fellowship. D.L. acknowledges support from the National Science Foundation under Cooperative Agreement No. PHY-2019786 (The NSF AI Institute for Artificial Intelligence and Fundamental Interactions [53]). L.F. was supported in part by a Simons Investigator Award from the Simons Foundation.

[1] S. M. Girvin and K. Yang, *Modern Condensed Matter Physics* (Cambridge University Press, Cambridge, U.K., 2019).

[2] P. Nozieres and D. Pines, *Theory Of Quantum Liquids*, Advanced Books Classics, 1st ed. (CRC Press, Boca Raton, 2000), p. 576.

[3] R. P. Feynman and M. Cohen, Energy spectrum of the excitations in liquid helium, Phys. Rev. **102**, 1189 (1956).

[4] Y. Onishi and L. Fu, Fundamental bound on topological gap, Phys. Rev. X **14**, 011052 (2024).

[5] Y. Onishi and L. Fu, Quantum weight: A fundamental property of quantum many-body systems, Phys. Rev. Res. **7**, 023158 (2025).

[6] B. Estienne, J. Stéphan, and W. Witczak-Krempa, Cornering the universal shape of fluctuations, Nat. Commun. **13**, 287 (2022).

[7] X.-C. Wu, K.-L. Cai, M. Cheng, and P. Kumar, Corner charge fluctuations and many-body quantum geometry, Phys. Rev. B **111**, 115124 (2025).

[8] X.-C. Wu, K.-L. Cai, M. Cheng, and P. Kumar, Corner charge fluctuations and many-body quantum geometry, arXiv:2408.16057.

[9] I. Souza, T. Wilkens, and R. M. Martin, Polarization and localization in insulators: Generating function approach, Phys. Rev. B **62**, 1666 (2000).

[10] I. Komissarov, T. Holder, and R. Queiroz, The quantum geometric origin of capacitance in insulators, Nat. Commun. **15**, 4621 (2024).

[11] I. Souza, R. M. Martin, and M. Stengel, Optical bounds on many-electron localization, SciPost Phys. **18**, 127 (2025).

[12] Y. Onishi and L. Fu, Topological bound on the structure factor, Phys. Rev. Lett. **133**, 206602 (2024).

[13] B. Ghosh, Y. Onishi, S.-Y. Xu, H. Lin, L. Fu, and A. Bansil, Probing quantum geometry through optical conductivity and magnetic circular dichroism, Sci. Adv. **10**, eado1761 (2024).

[14] N. Marzari and D. Vanderbilt, Maximally localized generalized Wannier functions for composite energy bands, Phys. Rev. B **56**, 12847 (1997).

[15] Q. Niu, D. J. Thouless, and Y.-S. Wu, Quantized Hall conductance as a topological invariant, Phys. Rev. B **31**, 3372 (1985).

[16] R. Roy, Band geometry of fractional topological insulators, Phys. Rev. B **90**, 165139 (2014).

[17] M. Claassen, C. H. Lee, R. Thomale, X.-L. Qi, and T. P. Devereaux, Position-momentum duality and fractional quantum Hall effect in Chern insulators, Phys. Rev. Lett. **114**, 236802 (2015).

[18] J. Wang, J. Cano, A. J. Millis, Z. Liu, and B. Yang, Exact Landau level description of geometry and interaction in a flatband, Phys. Rev. Lett. **127**, 246403 (2021).

[19] T. Ozawa and B. Mera, Relations between topology and the quantum metric for Chern insulators, Phys. Rev. B **104**, 045103 (2021).

[20] P. J. Ledwith, A. Vishwanath, and E. Khalaf, Family of ideal Chern flatbands with arbitrary Chern number in chiral twisted graphene multilayers, Phys. Rev. Lett. **128**, 176404 (2022).

[21] G. Shavit and Y. Oreg, Quantum geometry and stabilization of fractional Chern insulators far from the ideal limit, Phys. Rev. Lett. **133**, 156504 (2024).

[22] W.-X. Qiu and F. Wu, Quantum geometry probed by chiral excitonic optical response of Chern insulators, Phys. Rev. B **111**, L121104 (2025).

[23] D. Guerci, J. Wang, and C. Mora, Layer skyrmions for ideal Chern bands and twisted bilayer graphene, Phys. Rev. B (2025).

[24] F. Wu, T. Lovorn, E. Tutuc, I. Martin, and A. H. MacDonald, Topological insulators in twisted transition metal dichalcogenide homobilayers, Phys. Rev. Lett. **122**, 086402 (2019).

[25] T. Devakul, V. Crépel, Y. Zhang, and L. Fu, Magic in twisted transition metal dichalcogenide bilayers, Nat. Commun. **12**, 6730 (2021).

[26] H. Li, U. Kumar, K. Sun, and S.-Z. Lin, Spontaneous fractional Chern insulators in transition metal dichalcogenide moiré superlattices, Phys. Rev. Res. **3**, L032070 (2021).

[27] V. Crépel and L. Fu, Anomalous Hall metal and fractional Chern insulator in twisted transition metal dichalcogenides, Phys. Rev. B **107**, L201109 (2023).

[28] J. Cai, E. Anderson, C. Wang, X. Zhang, X. Liu, W. Holtzmann, Y. Zhang, F. Fan, T. Taniguchi, K. Watanabe *et al.*, Signatures of fractional quantum anomalous Hall states in twisted $MoTe_2$, Nature (London) **622**, 63 (2023).

[29] Y. Zeng, Z. Xia, K. Kang, J. Zhu, P. Knüppel, C. Vaswani, K. Watanabe, T. Taniguchi, K. F. Mak, and J. Shan, Thermodynamic evidence of fractional Chern insulator in moiré $MoTe_2$, Nature (London) **622**, 69 (2023).

[30] F. Xu, Z. Sun, T. Jia, C. Liu, C. Xu, C. Li, Y. Gu, K. Watanabe, T. Taniguchi, B. Tong, J. Jia, Z. Shi, S. Jiang, Y. Zhang, X. Liu, and T. Li, Observation of integer and fractional quantum anomalous Hall effects in twisted bilayer $MoTe_2$, Phys. Rev. X **13**, 031037 (2023).

[31] A. P. Reddy, F. Alsallom, Y. Zhang, T. Devakul, and L. Fu, Fractional quantum anomalous Hall states in twisted bilayer $MoTe_2$ and WSe_2, Phys. Rev. B **108**, 085117 (2023).

[32] C. Wang, X.-W. Zhang, X. Liu, Y. He, X. Xu, Y. Ran, T. Cao, and D. Xiao, Fractional Chern insulator in twisted bilayer $MoTe_2$, Phys. Rev. Lett. **132**, 036501 (2024).

[33] H. Goldman, A. P. Reddy, N. Paul, and L. Fu, Zero-field composite Fermi liquid in twisted semiconductor bilayers, Phys. Rev. Lett. **131**, 136501 (2023).

[34] J. Dong, J. Wang, P. J. Ledwith, A. Vishwanath, and D. E. Parker, Composite Fermi liquid at zero magnetic field in twisted $MoTe_2$, Phys. Rev. Lett. **131**, 136502 (2023).

[35] N. Morales-Durán, N. Wei, J. Shi, and A. H. MacDonald, Magic angles and fractional Chern insulators in twisted homobilayer transition metal dichalcogenides, Phys. Rev. Lett. **132**, 096602 (2024).

[36] V. Crépel, N. Regnault, and R. Queiroz, Chiral limit and origin of topological flat bands in twisted transition metal dichalcogenide homobilayers, Commun. Phys. **7**, 146 (2024).

[37] A. P. Reddy and L. Fu, Toward a global phase diagram of the fractional quantum anomalous Hall effect, Phys. Rev. B **108**, 245159 (2023).

[38] J. Yu, J. Herzog-Arbeitman, M. Wang, O. Vafek, B. A. Bernevig, and N. Regnault, Fractional Chern insulators versus nonmagnetic states in twisted bilayer $MoTe_2$, Phys. Rev. B **109**, 045147 (2024).

[39] A. Abouelkomsan, A. P. Reddy, L. Fu, and E. J. Bergholtz, Band mixing in the quantum anomalous Hall regime of twisted semiconductor bilayers, Phys. Rev. B **109**, L121107 (2024).

[40] J. Shi, N. Morales-Durán, E. Khalaf, and A. H. MacDonald, Adiabatic approximation and Aharonov-Casher bands in

twisted homobilayer transition metal dichalcogenides, Phys. Rev. B **110**, 035130 (2024).

[41] B. Li and F. Wu, Variational mapping of Chern bands to Landau levels: Application to fractional Chern insulators in twisted $MoTe_2$, Phys. Rev. B **111**, 125122 (2025).

[42] N. Morales-Durán, J. Wang, G. R. Schleder, M. Angeli, Z. Zhu, E. Kaxiras, C. Repellin, and J. Cano, Pressure-enhanced fractional Chern insulators along a magic line in moiré transition metal dichalcogenides, Phys. Rev. Res. **5**, L032022 (2023).

[43] P. Sharma, Y. Peng, and D. N. Sheng, Topological quantum phase transitions driven by a displacement field in twisted $MoTe_2$ bilayers, Phys. Rev. B **110**, 125142 (2024).

[44] H. Lu, H.-Q. Wu, B.-B. Chen, K. Sun, and Z. Y. Meng, Interaction-driven roton condensation in $C = 2/3$ fractional quantum anomalous Hall state, arXiv:2403.03258.

[45] D. N. Sheng, A. P. Reddy, A. Abouelkomsan, E. J. Bergholtz, and L. Fu, Quantum anomalous Hall crystal at fractional filling of moiré superlattices, Phys. Rev. Lett. **133**, 066601 (2024).

[46] C. Xu, J. Li, Y. Xu, Z. Bi, and Y. Zhang, Maximally localized Wannier functions, interaction models, and fractional quantum anomalous Hall effect in twisted bilayer $MoTe_2$, Proc. Natl. Acad. Sci. USA **121**, e2316749121 (2024).

[47] S. M. Girvin, A. H. MacDonald, and P. M. Platzman, Magneto-roton theory of collective excitations in the fractional quantum Hall effect, Phys. Rev. B **33**, 2481 (1986).

[48] T. Wolf, Y.-C. Chao, A. H. MacDonald, and J. J. Su, Intra-band collective excitations and spatial correlations in fractional Chern insulators, Phys. Rev. Lett. **134**, 116501 (2025).

[49] D. Mao, J. F. Mendez-Valderrama, and D. Chowdhury, Is the low-energy optical absorption in correlated insulators controlled by quantum geometry? arXiv:2410.16352.

[50] See Supplemental Material at http://link.aps.org/supplemental/10.1103/wlvf-tdq1 for explicit derivation for the full static structure factor within the continuum model for twisted TMDs while also detailing quantum geometry and quantum weight for interacting systems. We describe how we can extract the quantum weight directly from the full static structure factor. We provide additional data and calculations on Bragg peak scaling in addition to some extended data results.

[51] E. C. Regan, D. Wang, C. Jin, M. I. Bakti Utama, B. Gao, X. Wei, S. Zhao, W. Zhao, Z. Zhang, K. Yumigeta *et al.*, Mott and generalized Wigner crystal states in WSe_2/WS_2 moiré superlattices, Nature (London) **579**, 359 (2020).

[52] https://github.com/AidanReddy/FermionED.

[53] http://iaifi.org/.